Published in final edited form as:
Mol Cancer Ther. 2017 December ; 16(12): 2747–2758. doi:10.1158/1535-7163.MCT-17-0717.

Pharmacological dual inhibition of tumor and tumor-induced functional limitations in transgenic model of breast cancer

Ruizhong Wang[1], **Poornima Bhat-Nakshatri**[1], **Maria B Padua**[1], **Mayuri S Prasad**[1], **Manjushree Anjanappa**[1], **Max Jacobson**[2], **Courtney Finnearty**[2], **Victoria Sefcsik**[2], **Kyle McElyea**[2], **Rachael Redmond**[2], **George Sandusky**[2], **Narsimha Penthala**[3], **Peter A Crooks**[3], **Jianguo Liu**[1], **Teresa Zimmers**[1], and **Harikrishna Nakshatri**[1,4,5,*]

[1]Department of Surgery, Indiana University School of Medicine, Indianapolis, IN 46202, USA

[2]Department of Pathology and Laboratory Medicine, Indiana University School of Medicine, Indianapolis, IN 46202, USA

[3]Department of Pharmaceutical Sciences, College of Pharmacy, University of Arkansas for Medical Sciences, Little Rock, AK 72205, USA

[4]Department of Biochemistry and Molecular Biology, Indiana University School of Medicine, Indianapolis, IN 46202, USA

[5]Richard L Roudebush VA Medical Center, Indianapolis, IN 46202, USA

Abstract

Breast cancer progression is associated with systemic effects including functional limitations and sarcopenia without the appearance of overt cachexia. Autocrine/paracrine actions of cytokines/chemokines produced by cancer cells mediate cancer progression and functional limitations. The cytokine-inducible transcription factor NF-κB could be central to this process, as it displays oncogenic functions and is integral to the Pax7:MyoD:Pgc-1β:miR-486 myogenesis axis. We tested this possibility using the MMTV-PyMT transgenic mammary tumor model and the NF-κB inhibitor dimethylaminoparthenolide (DMAPT). We observed deteriorating physical and functional conditions in $PyMT^+$ mice with disease progression. Compared to wild type mice, tumor-bearing $PyMT^+$ mice showed decreased fat mass, impaired rotarod performance, and reduced grip strength as well as increased extracellular matrix (ECM) deposition in muscle. Contrary to acute cachexia models described in the literature, mammary tumor progression was associated with reduction in skeletal muscle stem/satellite-specific transcription factor Pax7. Additionally, we observed tumor-induced reduction in Pgc-1β in muscle, which controls mitochondrial biogenesis. DMAPT treatment starting at 6-8 weeks age prior to mammary tumor occurrence delayed mammary tumor onset and tumor growth rates without affecting metastasis. DMAPT overcame cancer-induced functional limitations and improved survival, which was accompanied with restoration of Pax7, Pgc-1β, and mitochondria levels and reduced ECM levels in skeletal muscles. In addition, DMAPT restored circulating levels of six out of 13 cancer-associated cytokines/chemokines changes to levels seen in healthy animals. These results reveal a

[*]Corresponding Author: Harikrishna Nakshatri, BVSc., PhD, C218C, 980 West Walnut St., Indianapolis, IN 46202, USA, 317 278 2238, hnakshat@iupui.edu.

pharmacological approach for overcoming cancer-induced functional limitations and the above noted cancer/drug-induced changes in muscle gene expression could be utilized as biomarkers of functional limitations.

Keywords

breast cancer; NF-κB; DMAPT; functional limitations; skeletal muscle

Introduction

Breast cancer is one of the most common cancers and a leading cause of cancer-associated morbidity/mortality in women worldwide (1). It is becoming increasingly clear that breast cancer is a systemic disease affecting multiple organs. The systemic effects of breast cancer are manifested in three distinct forms: functional limitation, sarcopenia, and cachexia (2-4). Functional Limitation, which is defined as muscle weakness and body pain with no obvious physical signs, is observed in 39% of breast cancer patients and is associated with increased risk of non-cancer cause of death (2). Functional limitation is found in women <40 ages even at the time of breast cancer diagnosis and before drug or surgical intervention (2,5). Sarcopenia (severe depletion of skeletal muscle, despite appearance of normal weight, overweight, or obesity) is observed in 25% of metastatic breast cancer patients and is associated with increased toxicity to chemotherapy (3). Additionally, 26% of breast cancer patients meet one of the four criteria of cachexia (4). Since onset of cachexia in breast cancer patients is not as rapid and progressive as in lung and pancreatic cancer, mechanistic studies on cachexia in breast cancer are limited. Acute cancer cachexia models used for mechanistic studies of cachexia in colon, pancreatic and lung cancers may not accurately reflect systemic impact of breast cancer. Therefore, model systems need to be developed to understand the systemic effects of functional limitations and sarcopenia in breast cancer and for the development of therapeutic strategies to treat these effects.

The main underlying pathophysiology of cancer-induced functional limitations/cachexia is thought involve the release of cytokines/chemokines such as tumor necrosis factor alpha (TNFα) and interleukin 1beta (IL-1β) from tumors that interfere with host immunity and skeletal muscle function (6). TNFα has been shown to impair muscle oxidative phenotype and cause muscle wasting (7). Thus, muscle wasting in advanced breast cancer may be due to potent catabolic effects of inflammatory cytokines through their downstream signaling. Muscle loss in cancer patients may be similar to age-associated muscle loss, which is accompanied with systemic inflammation and increased levels of cytokines including IL-1β, IL-6, IL-10, IL-13, TNFα and granulocyte-macrophage colony-stimulating factor (GM-CSF) (8). NF-κB is a major signaling molecule downstream of, and, in some cases, upstream of these cytokines (9). NF-κB is not only critical in tumor initiation and progression as demonstrated by us and others (9,10), but also regulates skeletal muscle mass and function by reducing protein synthesis or enhancing degradation of myogenic transcription factors such as MyoD (11). Activation of NF-κB through muscle-specific transgenic expression of activated IκB kinase beta (IKKβ) causes profound muscle wasting that resembles clinical cachexia (12). Therefore, NF-κB has been proposed to be a potential

target for the treatment of loss of skeletal muscle mass in cancer cachexia (11,13). However, most of the studies that examined the role of NF-κB in cancer cachexia were done using acute models of cachexia (~30 days) and it is yet to be ascertained whether these findings are relevant for breast cancer, which has a slower progression rate than other cancers, and usually does not display classic cachexia features.

Our previous study has shown that breast cancer patients with metastasis have lower level of circulating myogenic miR-486 (14). In line with human data, we observed that mice with mammary tumors have lower miR-486 concentrations in plasma and skeletal muscles (14). Mechanistic studies showed that tumor-induced cytokines such as TNFα and IL-1 are responsible for lower miR-486 expression in muscle cells. miR-486 is an integral part of a myogenesis signaling network that involves Pax7, MyoD, myostatin, and NF-κB (15-17) and MyoD actively induces its expression (17). In addition, miR-486 is essential for survival of cardiomyocytes since it blocks PTEN to upregulate PI3K/AKT (18). Furthermore, loss of miR-486 is a major defect in muscular dystrophy and transgenic expression of miR-486 in muscle can rescue muscular dystrophy phenotype in animal models (19). Considering the intricate network in muscle that involves both NF-κB and miR-486, this study aimed to determine whether pharmacological inhibition of NF-κB could overcome the cancer-induced musculoskeletal defects and expression of which among the genes within the broader NF-κB-Pax7-MyoD-miR-486 signaling axis could be restored in muscle upon pharmacological inhibition.

We employed MMTV-PyMT transgenic mice (called $PyMT^+$ mice hereafter) as an animal model of mammary tumors in order to characterize tumor progression and functional limitations (20). Genome-wide comparative analyses of multiple transgenic mammary tumor models have suggested $PyMT^+$ model to represent the luminal B intrinsic subtype of breast cancer (21). We used dimethylaminoparthenolide (DMAPT), a water-soluble analogue of parthenolide, which we have previously shown to have potent NF-κB inhibitory activity (22) and has been shown to overcome the adverse effects of persistent activation of NF-κB in BRCA1-deficient mammary luminal progenitor cells in vivo (23). We found that mammary tumor development in $PyMT^+$ mice was accompanied with functional limitations such as reduced grip strength, impaired rotarod balance, causing altered body composition as well as molecular changes in muscle including reduced expression of miR-486 and MyoD as we reported previously (14). Unlike in acute models of cachexia, which involves persistent expression of self-renewing factor Pax7 and block in myogenic differentiation (24), we observed lower Pax7 expression in muscle of $PyMT^+$ mice. We also observed reduced expression of peroxisome-activated receptor coactivator 1-beta (Pgc-1β) in skeletal muscle of $PyMT^+$ mice. MyoD, in combination with RelB, an alternative NF-κB, has been shown to maintain the expression of Pgc-1β in muscle and Pgc-1β is required for oxidative phosphorylation and mitochondrial biogenesis (25). DMAPT treatment ameliorates many of the functional limitations as well as the molecular changes in muscle including restoration of Pax7, MyoD, and Pgc-1β expression in muscle. These results have the potential for translation into a clinical strategy for targeting both tumors and functional limitations via inhibition of NF-κB to improve outcomes in breast cancer patients.

Materials and Methods

Transgenic mice, functional limitation studies and drug treatment

National Institutes of Health regulations concerning the use and care of experimental animals were followed while conducting animal studies and the Indiana University School of Medicine animal use committee approved this study. Male PyMT^{+} mice on a FVB/N background were purchased from Jackson Laboratory, and randomly bred with non-transgenic FVB/N females to obtain females heterozygous for the PyMT oncogene. Tumor progression was monitored periodically. Tumor volume was calculated as (length) × (width)^2/2. Echo-MRI (Houston, TX) was used to determine body compositions. Grip strength was measured by laying mice on a wire mesh connected to a test meter (Bioseb), and pulling the tail directly back parallel to the mesh surface, then recording the amount of force. Three trials of each test were performed with minimal 5 min intervals and the average value from the three recordings is presented. For rotarod performance (Harvard Apparatus), the period of time mice were able to remain on a rotating rod at 10 rpm was recorded 3 times at minimum 5 min intervals and the average from the three recordings is presented. For the drug intervention study, DMAPT (100 mg/kg) or vehicle (2.5% mannitol) was orally administrated to mice from Monday to Friday, starting 6-8 weeks post birth until the end of the experiment. Age-matched normal female mice were used as controls. Structure of DMAPT has been described previously (26). Blood and the tissues were collected at the time of sacrifice as per the recommendation of the attending veterinarian for miRNA, mRNA and protein preparation or for histological analysis. Drug treated animals were sacrificed at two different time points; one time point set at the same age as the control mice with tumors and the second set as recommended by the attending veterinarian to measure biochemical parameters.

Sample processing miRNA and total RNA extraction

Mouse blood was collected in a K2 EDTA coated tube, which was centrifuged at 2000 rpm for 15 min at 4°C. Immediately following centrifugation, supernatant was transferred into a clean Eppendorf tube for storage at -80°C. A Qiagen miRNeasy serum/plasma kit was used to isolate miRNA from 200 μL of stored plasma (Qiagen #217184). Tibialis anterior and gastrocnemius muscles from the hind limb of the mouse were harvested, snap-frozen and stored in -80°C. A Qiagen miRNeasy Mini Kit (#217004) or Qiagen RNeasy Mini Kit (#74106) was used to isolate miRNA or total RNA for RNA amplification from ~30 mgs of stored muscle. First, 700 μL QIAzol Lysis reagent/ or RLT lysis buffer was added to the tube containing dissected muscle, and the mixture then homogenized using a Qiagen TissueLyser LT unit with metal beads at a speed of 50Hz for 3 min, followed by 10 seconds sonication following the Qiagen recommended protocol.

Quantitative reverse transcription PCR

Five microliters of miRNAs extracted from plasma (20ng/μl) was used for cDNA synthesis using a Taqman miRNA Reverse Transcription Kit (Applied Biosystems). Total RNA from muscle tissues (200 ng/μl) were reverse transcribed into cDNAs using Bio-RAD iScript cDNA synthesis kit in a final volume of 20 μL. Quantitative PCR (qPCR) was performed using Taqman universal PCR mix (Applied Biosystems) and specific primers. miRNA

primers for U6 (#001973), miR-202 (#002579), miR-486 (#001278), miR-214 (#002293), miR-16 (#000391), miR-1(002222), miR-146a (000468), miR206 (#000510), and mRNA primers for Hsp90ab (#Mm00833431-g1), Pax7 (#Mm01354484-m1), MyoD (#Mm00440387-m1), Pgc-1β(#Mm00504730-m1), Acvr2b (#Mm00431664-m1), Dmpk(#Mm00446261-m1), Lmna(#Mm00497783-m1), Prkag1(#Mm00450298), Hoxa9 (#Mm00439364), Mt1 (#Mm00496660-g1) and Mt2 (#mm00809556-s1), were purchased from Applied Biosystems. Pgc-1β primers amplify exons 11 and 12 and measure only the "A" isoform of Pgc-1β. Each amplification reaction was performed in duplicate in a final volume of 20 μL with 4 μL of cDNA. The expression levels of miR-486 were normalized to miR-202 (mouse sera) and U6 (skeletal muscle) using the $2^{-\Delta\Delta Ct}$ method as described in a previous study (14).

Histological and immunohistochemical analysis

Tissues were immersed into 10% buffer formalin and stored in cold room. For H&E staining, formalin-fixed tissues were transferred to the pathology lab, paraffin-embedded, sliced, stained and analyzed by a pathologist. For immunofluorescence, formalin-fixed tissues were transferred to 20% sucrose in PBS over weekend, frozen, sliced with cryostat at 10 micron, mounted on positively-charged slides, then washed with PBS three times, and incubated with Cox IV antibody (Abcam #ab16056; 1:1000). The next day, sections were washed three times with PBS and subsequently incubated with secondary antibody conjugated with a fluorescent dyes. After a final wash with PBS, sections were sealed by mounting media with DAPI, and viewed under fluorescent microscope. For ECM histochemical examination, formalin-fixed, frozen sliced sections were washed with PBS three times and then incubated with Texas-red-conjugated-wheat germ agglutinin (WGA) (Invitrogen, #W21405, 1:1000). WGA staining was quantified to measure ECM area by using Image J software. The area occupied by WGA was expressed relative to total area of the muscle cross-section.

Western blotting

Freshly harvested or frozen mouse muscles (~30 mg tissue) was lysed in RIPA buffer with protease/phosphatase inhibitors (Sigma), then homogenized using Qiagen TissueLyser LT with metal beads at a speed of 50Hz for 3 min, followed by 10 seconds sonication. Thirty micrograms of proteins were used for Western blotting. Antibodies including mouse monoclonal Pax7 (Developmental Studies Hybridoma Bank, AB 528428) and MyoD (#sc-760, Santa Cruz Biotechnology) were used for Western blot analyses as per instructions from the manufacturers.

Cytokine measurements

Circulating cytokines were measured using 100μl of plasma and a MILLIPLEX MAP Mouse Cytokine/Chemokine Magnetic Bead Panel (MCYTMAG-70K-PX32, Millipore) that measures 32 cytokines/chemokines from limited samples. TGFβ1, 2 and 3 were measured separately. Each group contained plasma samples from six animals. Those samples with no detectable values were given a score of zero for the analyses.

Statistical analysis

Multiple group data were compared using ANOVA. A P value of <0.05 was considered statistically significant.

Results

Tumor progression in PyMT$^+$ transgenic mice is accompanied with functional limitations

PyMT$^+$ transgenic mice develop mammary tumors at 100% penetrance (20). Palpable tumors in females were evident as early as 60 days with a slow progression (by volume) for the first few days followed by rapid tumor growth requiring animal sacrifice due to humane reasons within 2-3 weeks following tumor occurrence. During an observation period from 8 to 14 weeks of age, we noted increased body weight in PyMT$^+$ mice compared to control mice (Fig. 1A), which was significant by 12 weeks. While PyMT$^+$ mice weighed 26±0.7grams, the weight of control mice at the same age was 23± 0.4 grams. By 14 weeks, differences became even more significant with tumor-bearing mice reaching 30±1.1 grams, whereas control mice remained at 23±0.4 grams (Fig. 1A). This weight gain in PyMT$^+$ mice is likely due to rapidly growing tumors.

We used echo-MRI to determine body composition. PyMT$^+$ mice had significant loss of body fat with progressive disease compared to control mice (Fig. 1B). For instance, the percentage of body fat was 15±1.3% at the age of eight weeks in PyMT$^+$ mice and significantly reduced to 10±0.5% at 14 weeks of age (Fig. 1B). In contrast to body fat, body lean mass increased with growth of tumors, and was particularly obvious at 14 weeks (Fig. 1C). Parallel to the changes in body lean mass, the percentage of body free water and body total water increased in PyMT$^+$ mice (Fig. 1D and 1E). This water retention may also have contributed to increased body weight in PyMT$^+$ mice and could be the result of tumor-induced impairment in lymphatic drainage. In line with body composition changes, we found that PyMT$^+$ mice had reduced grip strength (Fig.1F). Eight-week old PyMT$^+$ mice had 191±6.0 grams gripping force, which was further reduced to 162±6.6 grams and 162±2.7 grams gripping force by 12 and 14 weeks, respectively. The gripping force in FVB/N wild type mice remained ~200 grams during this observation period (Fig. 1F).

In order to test whether heart function was affected by mammary tumor burdens, we employed the ECGenie device to acquire ECG signals from live mice. Surprisingly, tumor burden did not significantly change heart beating intervals and heart beating rate (Supplementary Fig. 1). One reason for the lack of effects on cardiac function could be the rapid tumor growth forcing animal sacrifice before any cardiac effects of tumor burden were noticeable with available measurement tools.

DMAPT inhibits mammary tumors in PyMT$^+$ mice

To investigate whether NF-κB is the central node in cancer-induced systemic effects, we treated PyMT$^+$ mice with the NF-κB inhibitor DMAPT. DMAPT is a water-soluble analogue of parthenolide, an active ingredient of the herb feverfew (22,27). As with many targeted therapies, DMAPT displays NF-κB-dependent and NF-κB-independent activities; however, its major therapeutic effects are likely through NF-κB inhibition (22). Treatment

with DMAPT (100mg/kg, 5 times/week, orally), starting at 6-8 weeks of age, prior to visual appearance of mammary tumors, delayed mammary tumor visual onset and slowed tumor growth rates compared to vehicle treatment (Supplementary Table S1). At 10 weeks, 60% of $PyMT^+$ mice with vehicle treatment had developed mammary tumors, while only 10% of $PyMT^+$ mice with DMAPT treatment had mammary tumors. By 12 weeks, tumor burden was 3.6±1.2 cm^3 in mice treated with vehicle, while it was 0.7±0.3 cm^3 in mice with DMAPT treatment. These differences in tumor growth persisted until the termination of the study. Tumor burden was 10.6 ±1.6 cm^3 in mice treated with vehicle treatment vs. 6.3±1.3 cm^3 in mice treated with DMAPT by 14 weeks (Supplementary Table S1). Tumors of DMAPT-treated animals compared to tumors from vehicle-treated animals contained ~40% lower levels of transcripts for IL-6 ($p=0.006$), a NF-κB target gene, suggesting that the drug is targeting NF-κB in tumors. These differences in tumor growth/characteristics also translated into time of sacrifice of animals as recommended by the attending veterinarian. By this measurement, overall survival of animals in DMAPT treated group was significantly longer compared to control mice (Fig. 2A). For the purpose of tissue collection, we repeated the experiment with control and drug-treated groups and collected tissues at the same age point. Lungs from non-transgenic, $PyMT^+$, and $PyMT^+$ + DMAPT mice that were harvested at the same age as well as another group of control, untreated and drug-treated $PyMT^+$ animals, which were allowed to survive until recommended for euthanasia by the attending veterinarian, were examined for metastasis. Surprisingly, despite reduced tumor growth and improved survival, DMAPT-treated animals showed similar metastasis burden as untreated $PyMT^+$ mice (Fig. 2B). Note that all FVB/N background wild type mice did not develop mammary tumors during the entire period of these observations (Table S1).

DMAPT restores functional performance in $PyMT^+$ mice

We next examined function limitations including grip strength and rotarod performance. We observed that both vehicle and DMAPT treated mice had significantly lower gripping force to the metal wires of the test meter at 12 and 14 weeks of age compared to control mice. However, gripping force of DMAPT-treated mice was significantly better than vehicle-treated mice (Fig 3A). For instance, vehicle-treated mice had a gripping force of 159±3.9 g, while mice that received DMAPT had gripping force of 193±3.9 g. In addition, $PyMT^+$ mice that received DMAPT treatment had better rotarod performance. In the rotarod test, FVB/N wild type mice rotarod performance was 113±21 seconds, while $PyMT^+$ mice with vehicle could only hold on to the rotating rod for 11.6±2.7 seconds. DMAPT treated mice stayed on the rod for 37±9.7 seconds (Fig. 3B).

To examine whether DMAPT ameliorates alterations of body composition associated with mammary tumors in $PyMT^+$ mice, we monitored body weight, body fat, body lean mass, body free water, and body total water every other week utilizing echo-MRI analysis (Fig. 3C-3F). Both vehicle and DMAPT treated mice exhibited similar trend of changes in body composition in the three categories of body fat, body lean mass and total body water, but not in body free water (Fig. 3C-3F). There was a significant increase of body free water in mice treated with vehicle, but in mice treated with DMAPT body free water was significantly lower and similar to levels in non-transgenic wild type mice (Fig. 3E). In addition, DMAPT-treated mice gained less weight when compared to vehicle-treated mice (Fig. 3G).

Restoration of muscle function by DMAPT is accompanied with reversal of several cancer-induced molecular changes in skeletal muscle

To associate the beneficial effects of DMAPT with specific changes in molecular parameters, we measured the levels of skeletal-muscle enriched microRNAs in the circulation and in muscle. Consistent with our previous report (14), plasma miR-486 levels were lower in tumor-bearing mice compared to control mice (Fig. 4A). To our surprise, DMAPT treatment did not significantly restore circulating miR-486 levels despite improving muscle function. However, we found elevated levels of circulating miR-146a in animals treated with DMAPT. miR-146a, although NF-κB inducible, plays a major role in attenuating inflammation by targeting molecules in NF-κB regulatory network including cytokine receptors, thus reducing cytokine action and NF-κB activity (28).

We next examined miR-486 levels in muscles. miR-486 levels in the muscle of $PyMT^+$ mice were lower compared to control mice (Fig. 4B), similar to our previous observations (14). As with circulating miR-486, DMAPT-treatment did not restore muscle miR-486 (Fig. 4B). Thus, it appears that DMAPT restores muscle function that is independent of miR-486. miR-206 is another muscle-specific microRNA and inflammatory cytokines reduce its expression to promote muscle degeneration, inflammatory myopathies, and dermatomyositis (15,29,30). In addition, miR-206, secreted by myogenic progenitor cells, control extracellular matrix deposition (31). We measured miR-206 levels in muscle to further document the effects of cancer progression on muscle. Indeed, miR-206 levels in muscle were lower in $PyMT^+$ mice compared to control mice (Fig. 4B). Among other muscle-related microRNAs, we observed down-regulation of miR-214 but not miR-1 in skeletal muscle of $PyMT^+$ mice compared to control mice (Fig. 4B). Surprisingly, DMAPT failed to change the expression levels of any of these microRNAs. We noted that although circulating levels of miR-146a were elevated in DMAPT-treated animals, the levels did not change in muscle suggesting that muscle is not the source of circulating miR-146a in DMAPT-treated animals.

DMAPT restores loss of Pax7, MyoD, Hoxa9, and Pgc-1β in skeletal muscles of $PyMT^+$ mice

To determine whether enhanced functional performance upon DMAPT treatment can be correlated with the expression levels of other NF-κB targets, we first measured Pax7 protein levels in skeletal muscles. We found lower levels of Pax7 protein in muscle of $PyMT^+$ mice compared to wild type mice, and DMAPT restored Pax7 levels in tumor-bearing mice to levels similar to wild type mice (Fig. 5A). Consistent with protein analysis, qRT-PCR showed lower levels of Pax7 mRNA in $PyMT^+$ mice and the reverse in DMAPT-treated mice (Fig. 5B).

We also observed lower MyoD protein level in skeletal muscles of $PyMT^+$ mice compared to control mice although these differences did not reach statistical significance ($p=0.13$). However, MyoD protein levels in DMAPT treated animals were significantly higher than in untreated animals, suggesting that NF-κB inhibition can lead to elevated MyoD levels in muscle ($p=0.01$; Fig. 5A). As with protein levels, MyoD mRNA levels were lower in the muscle of $PyMT^+$ mice (Fig. 5B) but DMAPT treatment only marginally increased MyoD mRNA levels. Thus, it appears that DMAPT likely reduces MyoD protein turnover.

To identify additional targets of DMAPT, we performed Myogenesis and Myopathy PCR array (Qiagen) covering >90 muscle-enriched genes using skeletal muscle RNA from control, $PyMT^+$ and $PyMT^+$+DMAPT mice (n=5/group). Compared to control mice, only six genes in this panel showed significantly lower expression in muscle of $PyMT^+$ mice and none showed elevated expression (AcvR2b, Dmpk, Il-1β, Lmna, Nos2 and Prkag1, Supplemental Table S2). In DMAPT-treated mice, only Dmpk mRNA levels remained lower compared to control animals. In validation experiments, while AcvR2b, Dmpk, Lmna and Prkag1 mRNA levels remained low in the skeletal muscle of tumor-bearing animals, DMAPT failed to improve their expression levels. Thus, among myogenesis-associated genes, DMAPT was only able to restore the expression of only Pax7 and MyoD.

We examined the expression levels of four other genes associated with NF-κB signaling and are also recently been linked to metabolism, differentiation, and aging of muscle. These include Pgc-1β, which is induced by MyoD and alternate NF-κB, and is a negative regulator of canonical NF-κB signaling in skeletal muscle (25,32), Hoxa9, which is typically elevated in aging satellite cells of muscle and its expression is repressed by NF-κB (33,34), and metallothioneins 1 and 2 (Mt1 and Mt2), which control skeletal muscle mass and strength (35). Pgc-1β and Hoxa9 but Mt1 and Mt2 mRNA levels were lower in the skeletal muscle of tumor-bearing mice, which were reversed upon DMAPT treatment (Fig. 5B). Thus, DMAPT restored the expression of four proven targets of NF-κB in muscle (i.e. Pax7, MyoD, Pgc-1β, and Hoxa9).

DMAPT reverses cancer-induced loss in muscle mitochondria—Pgc-1β is necessary for oxidative phosphorylation and mitochondria biogenesis (25). Since Pgc-1β levels were lower in skeletal muscle of $PyMT^+$ mice, we next determined mitochondria content by staining for Cox IV, which is a mitochondria-enriched protein. Skeletal muscle of $PyMT^+$ mice contained lower levels of Cox IV compared to control mice and DMAPT treatment restored Cox IV levels (Fig. 6A). Thus, cancer-induced loss of Pgc-1β has an effect on mitochondria biogenesis in muscle, which may be a contributing factor for weakened muscle function.

DMAPT attenuates extracellular matrix deposition in skeletal muscles of $PyMT^+$ mice—The extracellular matrix (ECM) provides an appropriate and permissive environment for muscle development and functioning (36). Dynamic remodeling of the ECM is directed by the activity of matrix metalloproteinases such as MMP9, which is a known transcriptional target of NF-κB (37). Moreover, enhanced satellite cell to myogenic progenitor cell differentiation leads to increased ECM accumulation in muscle (31). Since muscle of tumor-bearing mice expressed low levels of the two satellite-specific transcription factors Pax7 and Hoxa9, which could be due to enhanced satellite cell to progenitor cell differentiation, we determined ECM composition in muscle. $PyMT^+$ mice had twice the level of ECM compared to control mice and this increase was blocked by DMAPT (Fig. 6B). Interestingly, H&E staining of muscles did not reveal morphological difference of muscle fibers and muscle fiber sizes among three groups under basic light microscope examination (Fig. 6C). Thus, cancer progressions in $PyMT^+$ mice is associated with molecular changes in

muscle, which may not be manifested at morphological levels but likely have consequential effects on muscle function.

DMAPT alters circulating cytokines/chemokines—We used a Bio-Plex 200 bead-based suspension system (Luminex platform) to determine tumor-induced changes in circulating cytokines/chemokines and to determine the effect of DMAPT treatment on their levels. Expression levels of seven (GM-CSF, TNFα, TGFβ2, TGFβ3, IL-6, VEGF, and G-CSF) were elevated and six (LIX, IL-1α, KC, IL-9, MIP-2, and TGFβ1) were decreased in $PyMT^+$ mice compared to control mice (Fig. 7, Supplementary Table S3 for raw data). DMAPT reversed cancer-induced changes in the expression of six of these cytokines (i.e. LIX, IL-1α, IL-9, MIP-2, TGFβ1, and GM-CSF). Among the cytokines whose expression was unaffected by tumors, DMAPT reduced the levels of IL-5 and MIP-1b. Collectively, these results demonstrate unique effects of PyMT-derived tumors on circulating cytokines/chemokines levels and pharmacologic approaches to circumvent these changes.

Discussion

Functional limitations and sarcopenia are the validated systemic effects of breast cancer (5,38). However, to our knowledge, none of the currently available transgenic models have been used to understand these systemic effects and to test for therapies that have dual effects on cancer and systemic effects or that may complement chemotherapy to improve quality of life. Numerous cachexia models have been developed over the years but most of these involve xenograft models with acute onset of cachexia (39,40). We initiated this study with three goals; 1) to determine whether transgenic models of breast cancer mimic functional limitations observed in patients; 2) If so, what are the molecular changes in muscle that accompany mammary tumor progression?; and 3) Can these models be used to identify therapies that might overcome systemic effects with or without anti-tumor effects. Our results clearly show that $PyMT^+$ mice develop functional limitations, which are accompanied with molecular changes in skeletal muscle, particularly the expression levels of satellite cell-specific transcription factors. Since many cancer patients experience parainflammation of epithelial origin and cytokines involved in this parainflammation can have paracrine effects on muscle (41), drugs that inhibit the function of cytokines could be effective in reducing cancer-associated systemic effects. The drug DMAPT inhibits NF-κB signaling downstream of many cytokines (22,27,42) and was effective in reducing systemic effects of mammary tumor. Although part of the benefits of DMAPT treatment on muscle function can be attributed to reduced tumor burden, we believe that the drug had additional direct effects on skeletal muscle. Untreated and DMAPT-treated mice showed similar metastatic burden, which indicates that the drug only limits the primary tumor growth and paracrine factors from metastasis that mediate systemic effects remain the same in untreated and drug-treated groups. In addition, circulating levels of several cytokines, particularly G-CSF, which promotes breast cancer metastasis through neutrophil polarization (43), were elevated in $PyMT^+$ mice and were unaffected by DMAPT treatment. The failure of DMAPT as a single agent to inhibit metastasis is not unexpected and is consistent with our previous report using parthenolide in xenograft models (44). However, the primary-tumor specific effect of the drug provides support for the recent observation that early dissemination seeds

metastasis and metastasis evolves independent of primary tumor with distinct signaling networks (45).

Genes that undergo changes in expression in cancer-associated skeletal muscle can be classified into two groups; one group of DMAPT-responsive genes that is integral to the NF-κB pathway, and the other DMAPT- insensitive group. The DMAPT-sensitive group included genes/proteins in the muscle satellite cell function including Pax7 and Hoxa9. We observed that the levels of both of these genes being lower in muscle of tumor-bearing mice compared to wild type mice. Hoxa9 deregulation in muscle has been studied in the context of aging but not functional limitation and the current study is the first report to show tumor-induced loss of Hoxa9 expression in muscle (33). Our observation on Pax7 depletion in the muscle of tumor-bearing transgenic mice is different from the observed accumulation of Pax7 in muscle under acute cachexia due to block in satellite cell differentiation (24). In this respect, the duration of the experiment may have contributed to these disparate results. The fact that both Pax7 and the other satellite factor Hoxa9 are reduced in muscle in our model clearly suggests that cancer advances aging of muscle. In this respect, we also observed increased circulating level of GM-CSF in $PyMT^+$ mice, which previously has been shown to mediate age-associated muscle loss in elderly patients (8). The reduction in MyoD and Pgc-1β in skeletal muscle of tumor-bearing mice is similar to reports in acute models of cachexia (46,47).

The set of down-regulated genes in skeletal muscle of $PyMT^+$ mice compared to wild type mice and that are insensitive to DMAPT include Acvr2b, Dmpk and Prkag1 and microRNAs miR-486 and miR-206. Activin type II receptor (Acvr2b) regulates skeletal muscle growth by binding with its ligands such as myostatin or activin (48). Myotonic dystrophy protein kinase (Dmpk) is a Ser/Thr protein kinase, mainly expressed in smooth, skeletal and cardiac muscles. Decreased Dmpk protein levels may contribute to the pathology of Myotonic Dystrophy, as revealed by gene targeting studies (49). Protein kinase AMP-activated non-catalytic subunit gamma 1 (Prkag1) is the regulatory subunit of AMP-activated protein kinase (AMPK), which is an important energy-sensing enzyme that monitors cellular energy status (50). Failure of DMAPT to restore the expression of these genes/microRNAs could be the reason for partial recovery of functional limitations and additional agents that restore the expression and/or function of these genes may provide better protection against cancer-induced systemic effects.

Our studies show that DMAPT had an effect outside the muscle tissue, which may have helped in reversing systemic effects of cancer and reversing NF-κB-driven inflammation. We observed elevated levels of miR-146a in the circulation but not in muscle of $PyMT^+$ mice treated with DMAPT. miR-146a attenuates the inflammatory response by targeting cytokine receptors that promote NF-κB-driven inflammation (51) and its upregulation in circulation of DMAPT-treated mice through an unknown mechanism and from an unknown source indicates treatment-induced attenuation of inflammation (28). Elevated miR-146a levels may also be responsible for restored muscle function in DMAPT-treated mice despite the failure of the drug to reduce the levels of pro-inflammatory cytokines such as TNFα, IL-6, TGFβ2, TGFβ3, and G-CSF, many of which have been linked to cancer-induced changes in skeletal muscle function in at least in vitro studies (39). These results also

highlight the difficulty in translating results from in vitro studies that show the effect of these cytokines on skeletal muscle differentiation into the in vivo condition.

In summation, this report documents skeletal muscle changes in a chronic mammary tumor model that represents a luminal B intrinsic subtype of breast cancer that are partially different from changes observed in acute tumor/cachexia models, and the feasibility of reversing these changes by utilizing drugs with NF-κB inhibitory activity. Circulating miR-146a and GM-CSF levels as well as expression levels of Pax7, Hoxa9, MyoD, Pgc-1β and Cox IV in muscle could be used as biomarkers to document cancer-induced functional limitations and the specificity of drugs that overcome functional limitations.

Supplementary Material

Refer to Web version on PubMed Central for supplementary material.

Acknowledgments

We thank immunohistochemistry core for tissue staining and the Multiplex Analysis Core at the Indiana University Melvin and Bren Simon Cancer Center for providing support for analyzing plasma samples.

Funding: Department of Veterans Affairs merit award BX002764 funded this study (to HN). MBP was supported by a fellowship from the Vera Bradley Foundation for Breast Cancer Research.

References

1. Shachar SS, Deal AM, Weinberg M, Nyrop KA, Williams GR, Nishijima TF, et al. Skeletal Muscle Measures as Predictors of Toxicity, Hospitalization, and Survival in Patients with Metastatic Breast Cancer Receiving Taxane-Based Chemotherapy. Clin Cancer Res. 2017; 23(3):658–65. [PubMed: 27489287]
2. Kroenke CH, Rosner B, Chen WY, Kawachi I, Colditz GA, Holmes MD. Functional impact of breast cancer by age at diagnosis. J Clin Oncol. 2004; 22(10):1849–56. [PubMed: 15143077]
3. Prado CM, Baracos VE, McCargar LJ, Reiman T, Mourtzakis M, Tonkin K, et al. Sarcopenia as a determinant of chemotherapy toxicity and time to tumor progression in metastatic breast cancer patients receiving capecitabine treatment. Clin Cancer Res. 2009; 15(8):2920–6. [PubMed: 19351764]
4. Fox KM, Brooks JM, Gandra SR, Markus R, Chiou CF. Estimation of Cachexia among Cancer Patients Based on Four Definitions. Journal of oncology. 2009; 2009:693458. [PubMed: 19587829]
5. Braithwaite D, Satariano WA, Sternfeld B, Hiatt RA, Ganz PA, Kerlikowske K, et al. Long-term prognostic role of functional limitations among women with breast cancer. J Natl Cancer Inst. 2010; 102(19):1468–77. [PubMed: 20861456]
6. Patel HJ, Patel BM. TNF-alpha and cancer cachexia: Molecular insights and clinical implications. Life Sci. 2017; 170:56–63. [PubMed: 27919820]
7. Remels AH, Gosker HR, Schrauwen P, Hommelberg PP, Sliwinski P, Polkey M, et al. TNF-alpha impairs regulation of muscle oxidative phenotype: implications for cachexia? FASEB J. 2010; 24(12):5052–62. [PubMed: 20807714]
8. Calvani R, Marini F, Cesari M, Buford TW, Manini TM, Pahor M, et al. Systemic inflammation, body composition, and physical performance in old community-dwellers. J Cachexia Sarcopenia Muscle. 2017; 8(1):69–77. [PubMed: 27897412]
9. Perkins ND. The diverse and complex roles of NF-kappaB subunits in cancer. Nat Rev Cancer. 2012; 12(2):121–32. [PubMed: 22257950]
10. Nakshatri H, Bhat-Nakshatri P, Martin DA, Goulet RJ Jr, Sledge GW Jr. Constitutive activation of NF-kappaB during progression of breast cancer to hormone-independent growth. Mol Cell Biol. 1997; 17(7):3629–39. [PubMed: 9199297]

11. Bakkar N, Guttridge DC. NF-kappaB signaling: a tale of two pathways in skeletal myogenesis. Physiol Rev. 2010; 90(2):495–511. [PubMed: 20393192]
12. Cai D, Frantz JD, Tawa NE Jr, Melendez PA, Oh BC, Lidov HG, et al. IKKbeta/NF-kappaB activation causes severe muscle wasting in mice. Cell. 2004; 119(2):285–98. [PubMed: 15479644]
13. Chacon-Cabrera A, Fermoselle C, Urtreger AJ, Mateu-Jimenez M, Diament MJ, de Kier Joffe ED, et al. Pharmacological strategies in lung cancer-induced cachexia: effects on muscle proteolysis, autophagy, structure, and weakness. J Cell Physiol. 2014; 229(11):1660–72. [PubMed: 24615622]
14. Chen D, Goswami CP, Burnett RM, Anjanappa M, Bhat-Nakshatri P, Muller W, et al. Cancer Affects microRNA Expression, Release, and Function in Cardiac and Skeletal Muscle. Cancer Res. 2014; 74:4270–81. [PubMed: 24980554]
15. Horak M, Novak J, Bienertova-Vasku J. Muscle-specific microRNAs in skeletal muscle development. Dev Biol. 2016; 410(1):1–13. [PubMed: 26708096]
16. Dey BK, Gagan J, Dutta A. miR-206 and -486 induce myoblast differentiation by downregulating Pax7. Mol Cell Biol. 2011; 31(1):203–14. [PubMed: 21041476]
17. Buckingham M, Rigby PW. Gene Regulatory Networks and Transcriptional Mechanisms that Control Myogenesis. Dev Cell. 2014; 28(3):225–38. [PubMed: 24525185]
18. Small EM, O'Rourke JR, Moresi V, Sutherland LB, McAnally J, Gerard RD, et al. Regulation of PI3-kinase/Akt signaling by muscle-enriched microRNA-486. Proc Natl Acad Sci U S A. 2010; 107(9):4218–23. [PubMed: 20142475]
19. Alexander MS, Casar JC, Motohashi N, Vieira NM, Eisenberg I, Marshall JL, et al. MicroRNA-486-dependent modulation of DOCK3/PTEN/AKT signaling pathways improves muscular dystrophy-associated symptoms. J Clin Invest. 2014; 124(6):2651–67. [PubMed: 24789910]
20. Lin EY, Jones JG, Li P, Zhu L, Whitney KD, Muller WJ, et al. Progression to malignancy in the polyoma middle T oncoprotein mouse breast cancer model provides a reliable model for human diseases. Am J Pathol. 2003; 163(5):2113–26. [PubMed: 14578209]
21. Pfefferle AD, Herschkowitz JI, Usary J, Harrell JC, Spike BT, Adams JR, et al. Transcriptomic classification of genetically engineered mouse models of breast cancer identifies human subtype counterparts. Genome Biol. 2013; 14(11):R125. [PubMed: 24220145]
22. Nakshatri H, Appaiah HN, Anjanappa M, Gilley D, Tanaka H, Badve S, et al. NF-kappaB-dependent and -independent epigenetic modulation using the novel anti-cancer agent DMAPT. Cell death & disease. 2015; 6:e1608. [PubMed: 25611383]
23. Sau A, Lau R, Cabrita MA, Nolan E, Crooks PA, Visvader JE, et al. Persistent Activation of NF-kappaB in BRCA1-Deficient Mammary Progenitors Drives Aberrant Proliferation and Accumulation of DNA Damage. Cell Stem Cell. 2016; 19(1):52–65. [PubMed: 27292187]
24. He WA, Berardi E, Cardillo VM, Acharyya S, Aulino P, Thomas-Ahner J, et al. NF-kappaB-mediated Pax7 dysregulation in the muscle microenvironment promotes cancer cachexia. J Clin Invest. 2013; 123(11):4821–35. [PubMed: 24084740]
25. Shintaku J, Peterson JM, Talbert EE, Gu JM, Ladner KJ, Williams DR, et al. MyoD Regulates Skeletal Muscle Oxidative Metabolism Cooperatively with Alternative NF-kappaB. Cell reports. 2016; 17(2):514–26. [PubMed: 27705798]
26. Neelakantan S, Nasim S, Guzman ML, Jordan CT, Crooks PA. Aminoparthenolides as novel anti-leukemic agents: Discovery of the NF-kappaB inhibitor, DMAPT (LC-1). Bioorg Med Chem Lett. 2009; 19(15):4346–9. [PubMed: 19505822]
27. Shanmugam R, Kusumanchi P, Appaiah H, Cheng L, Crooks P, Neelakantan S, et al. A water soluble parthenolide analog suppresses in vivo tumor growth of two tobacco-associated cancers, lung and bladder cancer, by targeting NF-kappaB and generating reactive oxygen species. Int J Cancer. 2011; 128(10):2481–94. [PubMed: 20669221]
28. Taganov KD, Boldin MP, Chang KJ, Baltimore D. NF-kappaB-dependent induction of microRNA miR-146, an inhibitor targeted to signaling proteins of innate immune responses. Proc Natl Acad Sci U S A. 2006; 103(33):12481–6. [PubMed: 16885212]
29. Georgantas RW, Streicher K, Greenberg SA, Greenlees LM, Zhu W, Brohawn PZ, et al. Inhibition of myogenic microRNAs 1, 133, and 206 by inflammatory cytokines links inflammation and

muscle degeneration in adult inflammatory myopathies. Arthritis Rheumatol. 2014; 66(4):1022–33. [PubMed: 24757153]

30. Tang X, Tian X, Zhang Y, Wu W, Tian J, Rui K, et al. Correlation between the frequency of Th17 cell and the expression of microRNA-206 in patients with dermatomyositis. Clin Dev Immunol. 2013; 2013:345347. [PubMed: 24288551]
31. Fry CS, Kirby TJ, Kosmac K, McCarthy JJ, Peterson CA. Myogenic Progenitor Cells Control Extracellular Matrix Production by Fibroblasts during Skeletal Muscle Hypertrophy. Cell Stem Cell. 2017; 20(1):56–69. [PubMed: 27840022]
32. Eisele PS, Salatino S, Sobek J, Hottiger MO, Handschin C. The peroxisome proliferator-activated receptor gamma coactivator 1alpha/beta (PGC-1) coactivators repress the transcriptional activity of NF-kappaB in skeletal muscle cells. J Biol Chem. 2013; 288(4):2246–60. [PubMed: 23223635]
33. Schworer S, Becker F, Feller C, Baig AH, Kober U, Henze H, et al. Epigenetic stress responses induce muscle stem-cell ageing by Hoxa9 developmental signals. Nature. 2016; 540(7633):428–32. [PubMed: 27919074]
34. Trivedi CM, Patel RC, Patel CV. Differential regulation of HOXA9 expression by nuclear factor kappa B (NF-kappaB) and HOXA9. Gene. 2008; 408(1-2):187–95. [PubMed: 18068911]
35. Summermatter S, Bouzan A, Pierrel E, Melly S, Stauffer D, Gutzwiller S, et al. Blockade of Metallothioneins 1 and 2 Increases Skeletal Muscle Mass and Strength. Mol Cell Biol. 2017; 37(5)
36. Calve S, Odelberg SJ, Simon HG. A transitional extracellular matrix instructs cell behavior during muscle regeneration. Dev Biol. 2010; 344(1):259–71. [PubMed: 20478295]
37. Hatfield KJ, Reikvam H, Bruserud O. The crosstalk between the matrix metalloprotease system and the chemokine network in acute myeloid leukemia. Curr Med Chem. 2010; 17(36):4448–61. [PubMed: 21062258]
38. Pardo I, Lillemoe HA, Blosser RJ, Choi M, Sauder CA, Doxey DK, et al. Next-generation transcriptome sequencing of the premenopausal breast epithelium using specimens from a normal human breast tissue bank. Breast Cancer Res. 2014; 16(2):R26. [PubMed: 24636070]
39. Miyamoto Y, Hanna DL, Zhang W, Baba H, Lenz HJ. Molecular Pathways: Cachexia Signaling-A Targeted Approach to Cancer Treatment. Clin Cancer Res. 2016; 22(16):3999–4004. [PubMed: 27340276]
40. Ballaro R, Costelli P, Penna F. Animal models for cancer cachexia. Curr Opin Support Palliat Care. 2016; 10(4):281–87. [PubMed: 27454355]
41. Aran D, Lasry A, Zinger A, Biton M, Pikarsky E, Hellman A, et al. Widespread parainflammation in human cancer. Genome Biol. 2016; 17(1):145. [PubMed: 27386949]
42. Guzman ML, Rossi RM, Neelakantan S, Li X, Corbett CA, Hassane DC, et al. An orally bioavailable parthenolide analog selectively eradicates acute myelogenous leukemia stem and progenitor cells. Blood. 2007; 110(13):4427–35. [PubMed: 17804695]
43. Coffelt SB, Kersten K, Doornebal CW, Weiden J, Vrijland K, Hau CS, et al. IL-17-producing gammadelta T cells and neutrophils conspire to promote breast cancer metastasis. Nature. 2015; 522(7556):345–8. [PubMed: 25822788]
44. Sweeney CJ, Mehrotra S, Sadaria MR, Kumar S, Shortle NH, Roman Y, et al. The sesquiterpene lactone parthenolide in combination with docetaxel reduces metastasis and improves survival in a xenograft model of breast cancer. Mol Cancer Ther. 2005; 4(6):1004–12. [PubMed: 15956258]
45. Hosseini H, Obradovic MM, Hoffmann M, Harper KL, Sosa MS, Werner-Klein M, et al. Early dissemination seeds metastasis in breast cancer. Nature. 2016; doi: 10.1038/nature20785
46. Guttridge DC, Mayo MW, Madrid LV, Wang CY, Baldwin AS Jr. NF-kappaB-induced loss of MyoD messenger RNA: possible role in muscle decay and cachexia. Science. 2000; 289(5488): 2363–6. [see comments]. [PubMed: 11009425]
47. Sacheck JM, Hyatt JP, Raffaello A, Jagoe RT, Roy RR, Edgerton VR, et al. Rapid disuse and denervation atrophy involve transcriptional changes similar to those of muscle wasting during systemic diseases. FASEB J. 2007; 21(1):140–55. [PubMed: 17116744]
48. Zhou X, Wang JL, Lu J, Song Y, Kwak KS, Jiao Q, et al. Reversal of cancer cachexia and muscle wasting by ActRIIB antagonism leads to prolonged survival. Cell. 2010; 142(4):531–43. [PubMed: 20723755]

49. Kaliman P, Llagostera E. Myotonic dystrophy protein kinase (DMPK) and its role in the pathogenesis of myotonic dystrophy 1. Cell Signal. 2008; 20(11):1935–41. [PubMed: 18583094]

50. Schonke M, Myers MG Jr, Zierath JR, Bjornholm M. Skeletal muscle AMP-activated protein kinase gamma1(H151R) overexpression enhances whole body energy homeostasis and insulin sensitivity. American journal of physiology Endocrinology and metabolism. 2015; 309(7):E679–90. [PubMed: 26306597]

51. Li K, Ching D, Luk FS, Raffai RL. Apolipoprotein E enhances microRNA-146a in monocytes and macrophages to suppress nuclear factor-kappaB-driven inflammation and atherosclerosis. Circulation research. 2015; 117(1):e1–e11. [PubMed: 25904598]

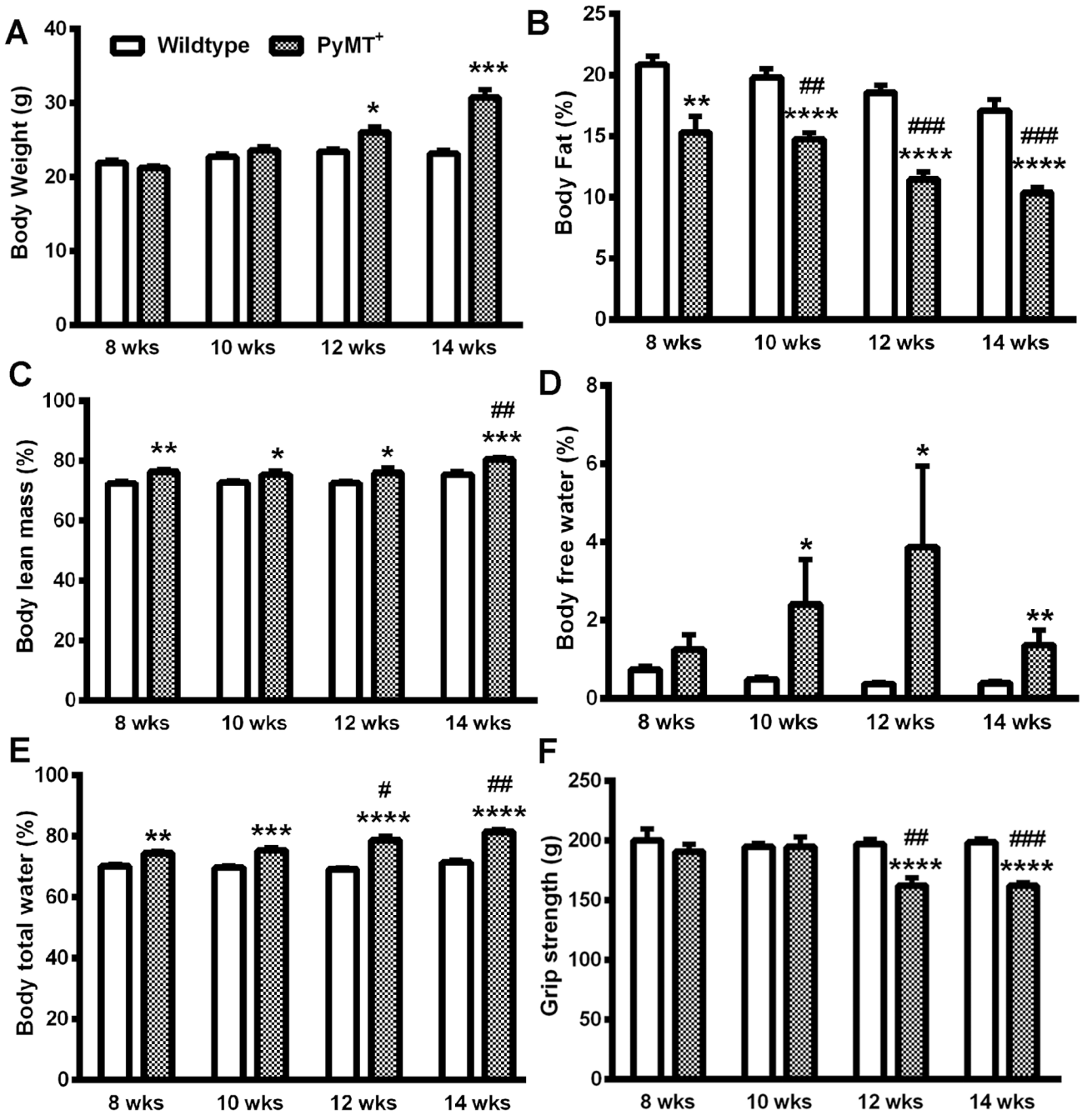

Figure 1.

Characterization of systemic effects of mammary tumors in PyMT$^+$ mice. A) Body weight. B) Percentage of fat over total body weight. C) Percentage of lean mass over total body weight. D) Percentage of body free water over total body weight. E) Percentage of total body water over total body weight. F) Grip strength. * indicates significance between PyMT$^+$ and wild type groups, $p<0.05$. # indicates significance between baseline (eight weeks) and experimental data from the same group, $p<0.05$. n= 5 (wild type) and 8 (PyMT$^+$) mice/group.

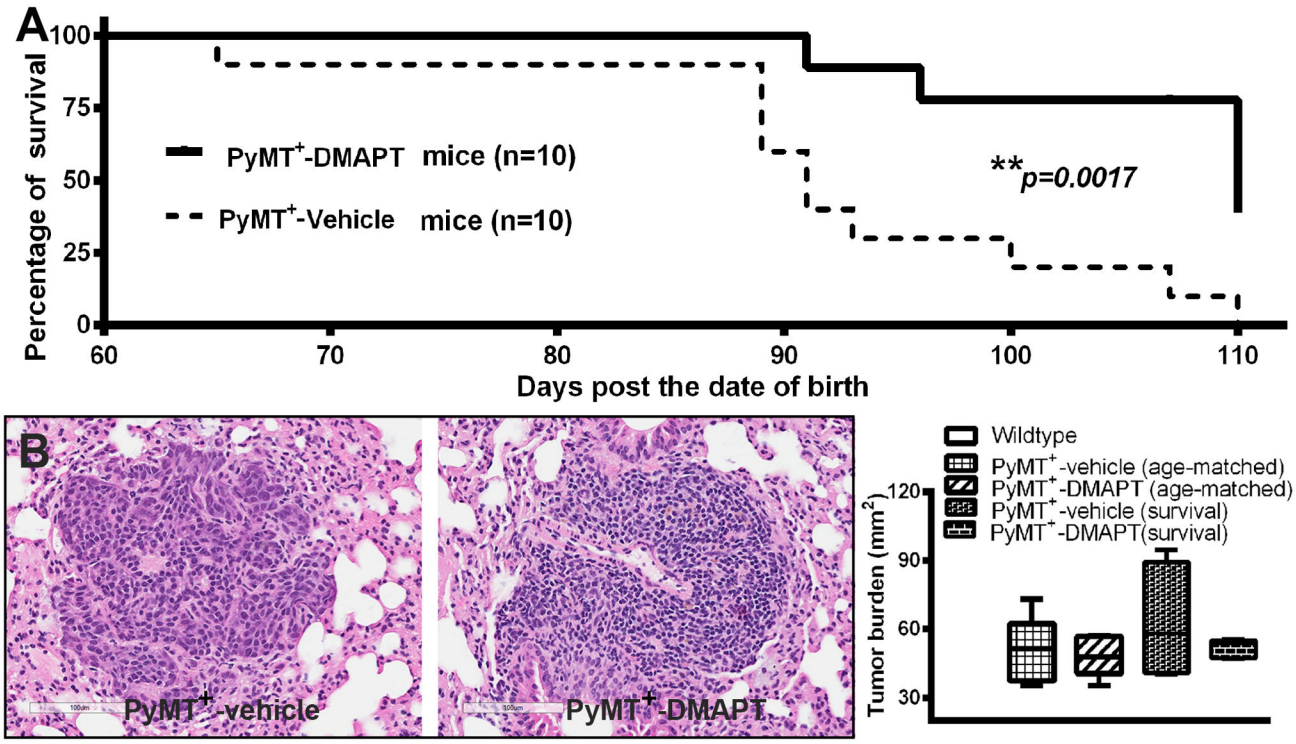

Figure 2.

The effect of DMAPT on survival and metastasis. A) Oral administration of DMAPT (100mg/kg, M-F/week, starting at 6-8 weeks age) improves survival. (B) Left panel images show representative lung metastasis and right graph shows average lung metastasis area per mouse. n=5 mice/group. Note that this analysis included two sets of mice; lungs from age-matched untreated and DMAPT-treated animals and from animals collected at the end of the terminal experiments. In both sets, there were no statistical differences in rate of metastasis between groups, although there was a trend of lower metastasis in the DMAPT-treated group.

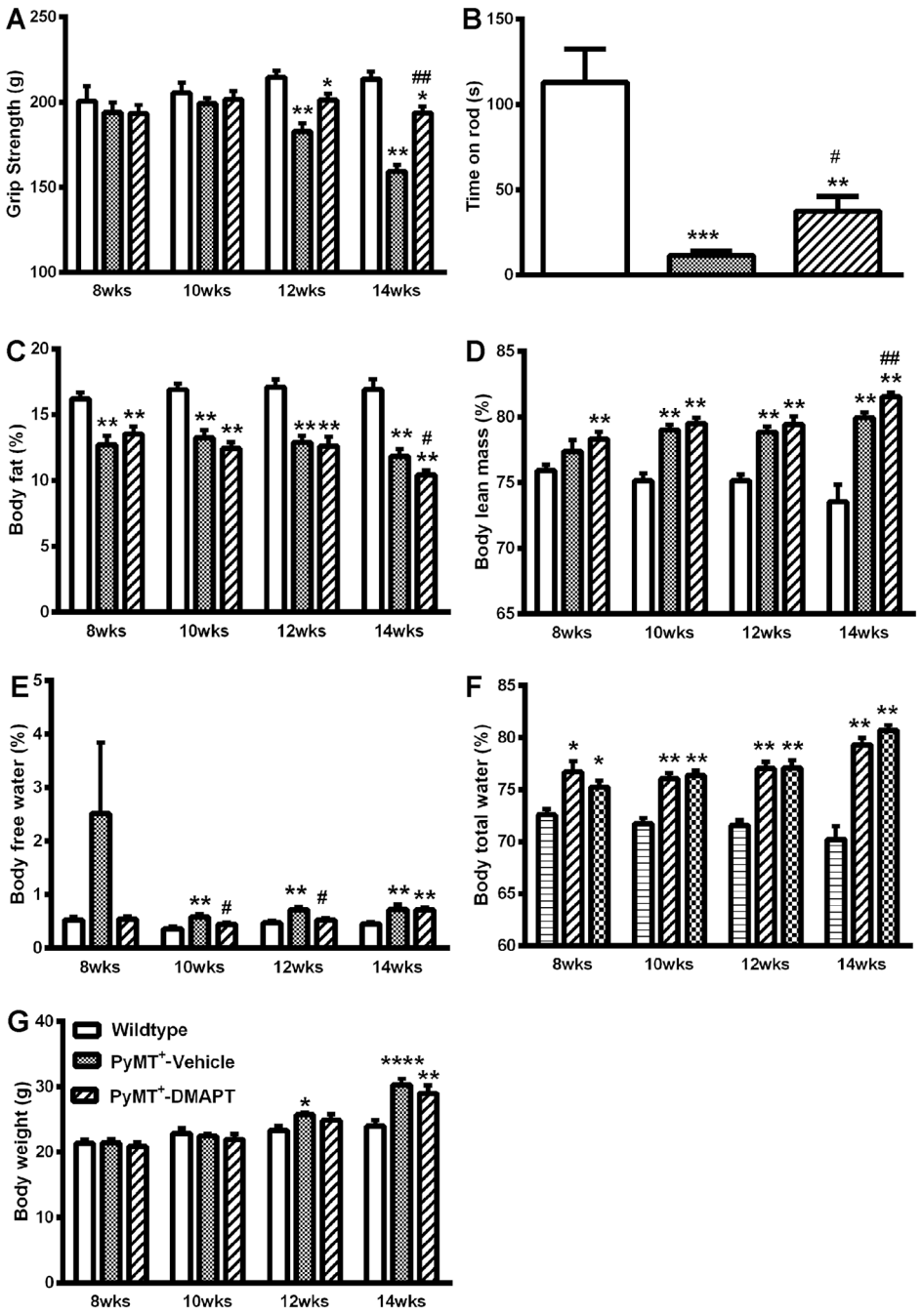

Figure 3.

Oral administration of DMAPT (100mg/kg, M-F/week) modulates body composition and functional performance in PyMT^{+} mice. A) DMAPT restores grip strength. B) DMAPT partially ameliorates tumor-induced decline in rotarod performance. C) DMAPT treatment does not alter tumor-induced loss of fat. D) DMAPT has minimal effect on tumor-induced changes in body lean mass. E) DMAPT reduces percentage of body free water. F) DMAPT does not significantly change total body water ratio. g) DMAPT slows down body weight gain. * indicates significance between experimental groups and wild type group, $p<0.05$. #

indicates significance between PyMT^{+} group with vehicle and with DMAPT treatments at same age-testing point, $p<0.05$. n= 10 mice/group.

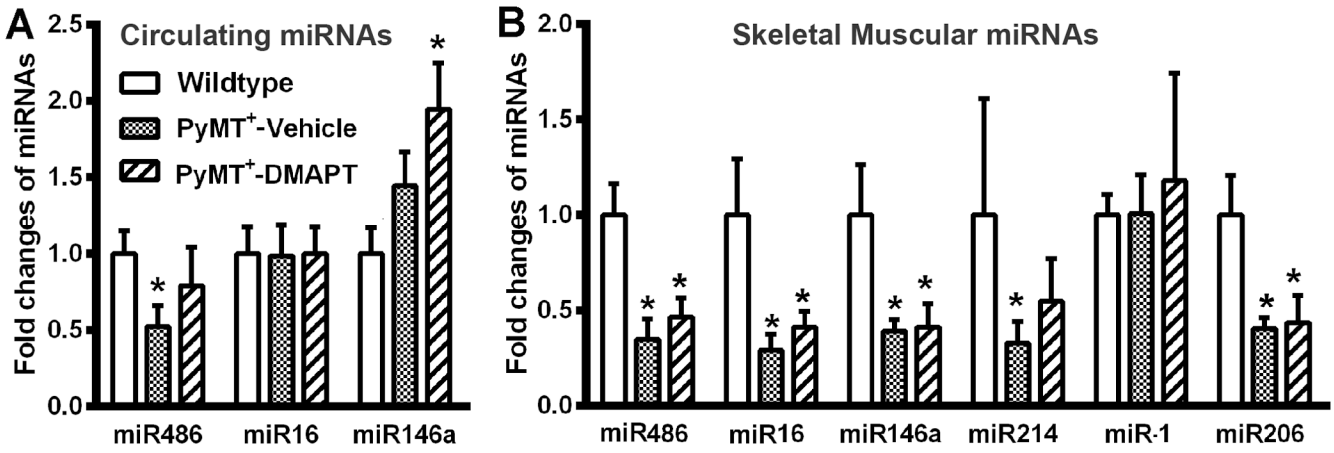

Figure 4.

The effect of DMAPT on cancer-induced changes in circulating and muscle-enriched microRNAs. A) The effect of DMAPT on circulating miRNAs. miR-486 levels were lower in plasma of $PyMT^+$ mice, which remained low in DMAPT-treated mice. DMAPT increased circulating miR-146a levels. B). DMAPT treatment did not restore tumor-induced loss of muscle-enriched microRNAs in hind limb muscle of $PyMT^+$ mice. Average and standard deviation are shown. * indicates significance between experimental and wild type groups, $p<0.05$. n= 8-10 mice/group.

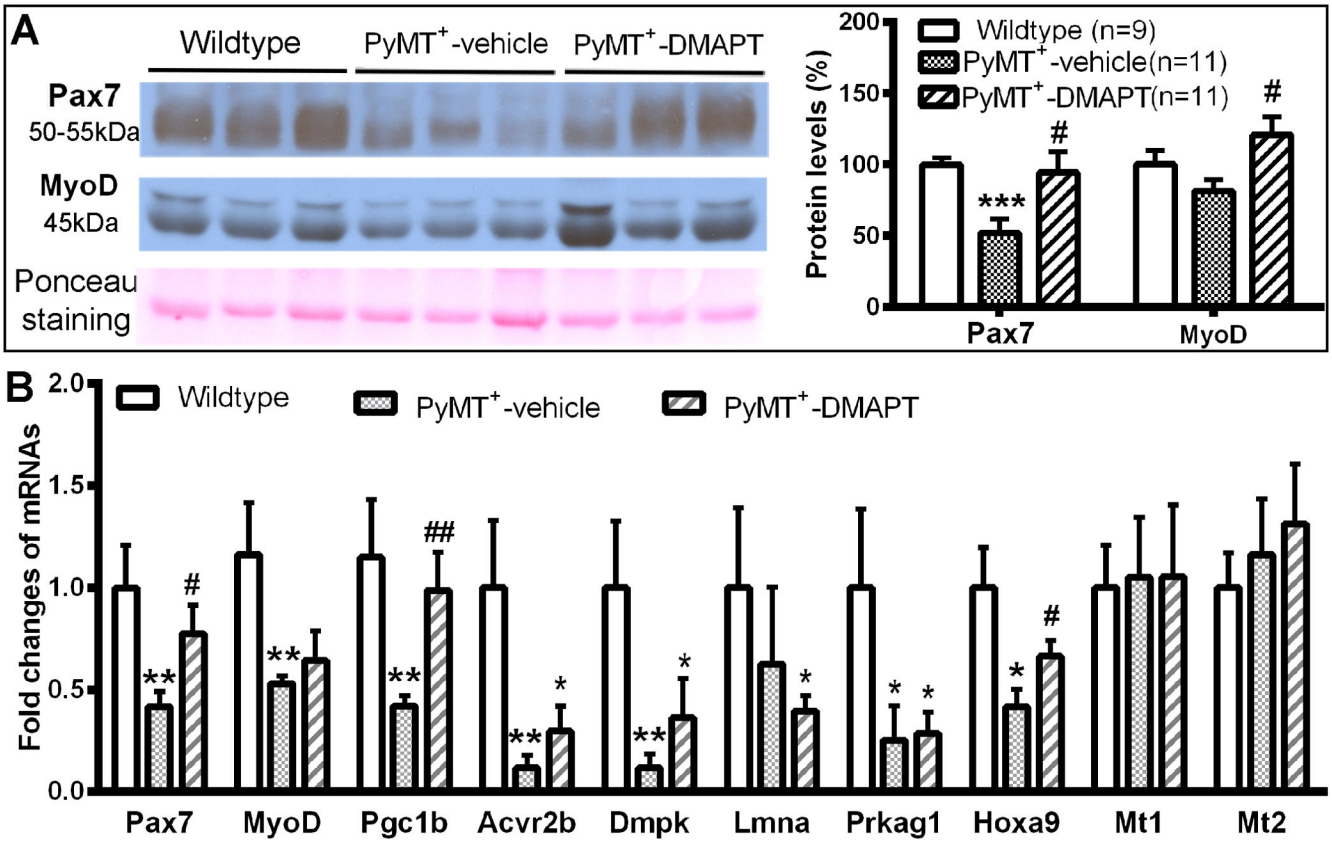

Figure 5.

DMAPT restores tumor-induced loss of Pax7, MyoD and Pgc-1β in skeletal muscle. A) Pax7 and MyoD protein levels. Left panel images show Pax7 and MyoD protein in skeletal muscles of hind limbs. Image J was used to quantitate Western blotting data (right panel). B) qRT-PCR analysis of multiple mRNAs in skeletal muscles of PyMT$^+$ mice. Eight of 10 analyzed mRNAs are downregulated in muscle whereas two of 10 mRNAs are not changed in PyMT$^+$ mice compared to wild type mice. DMAPT treatment significantly reversed tumor-induced loss of Pax7, Pgc-1β and Hoxa9 mRNA levels. * indicates significance between experimental and wild type groups, $p<0.05$. # indicates significance between vehicle-treated and DMAPT-treated PyMT$^+$ animals. $p<0.05$. n= 8-10 mice/group.

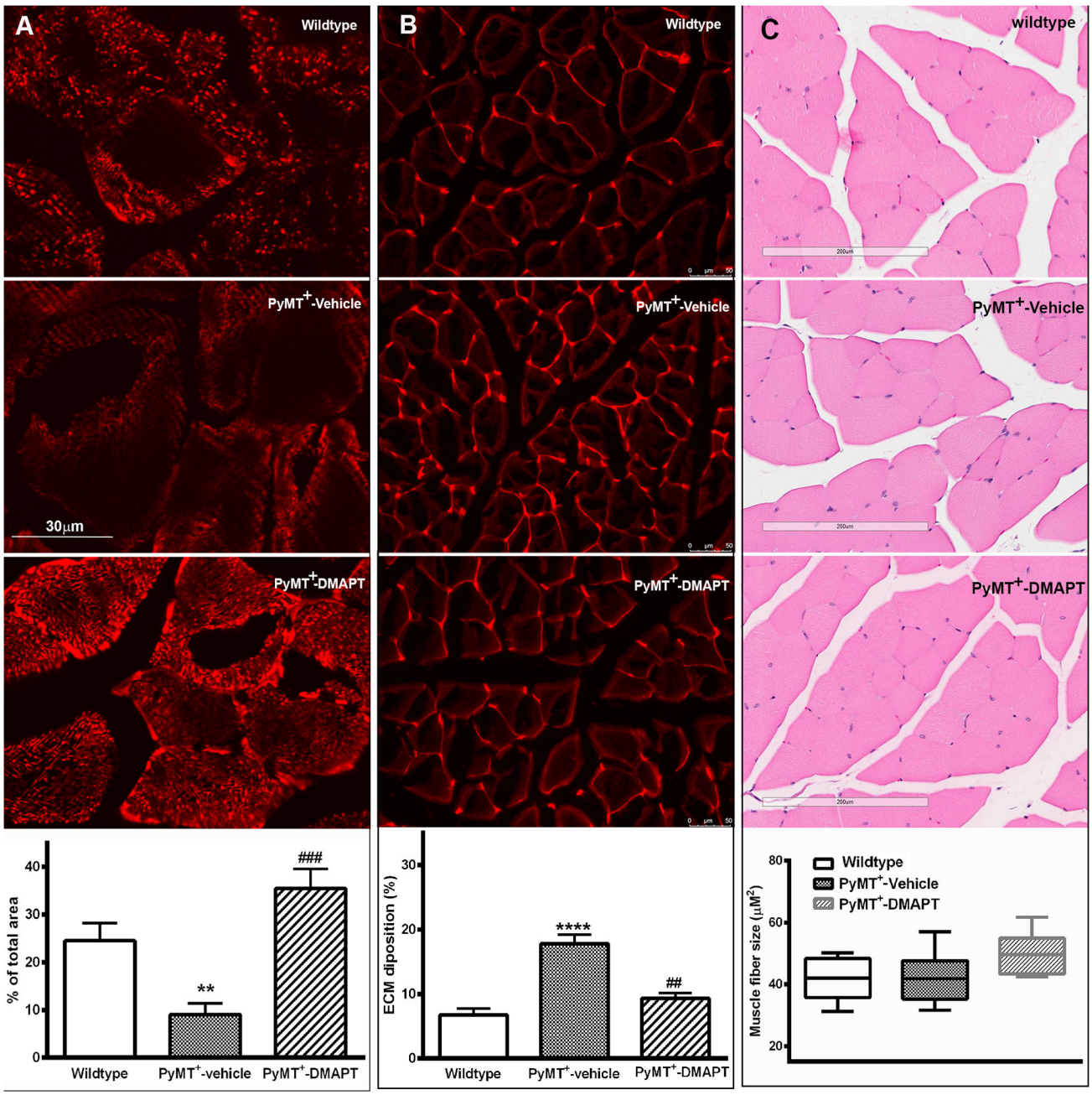

Figure 6.

Cox IV, ECM, and muscle fiber length changes in skeletal muscle of transgenic mice. A) Cox IV levels, a Pgc-1β target, in muscle. Cox IV levels were measured by immunofluorescence and quantitated using Image J. B) Deposition of extracellular Matrix (ECM) in skeletal muscle of $PyMT^{+}$ mice. Top images show histochemical staining by Texas-red-conjugated-wheat germ agglutinin in skeletal muscle of mice, whereas bottom graph shows quantification of ECM by Image J. C) Analysis of skeletal muscle in hind limb of mice. Top images show H&E staining of quadriceps, whereas bottom graph shows analysis of average area of cross section of each skeletal muscle fiber from quadriceps. *

indicates significance between experimental and wild type groups, $p<0.05$. # indicates significance between vehicle-treated and DMAPT-treated PyMT^{+} animals. $p<0.05$. n= 5-6 mice/group.

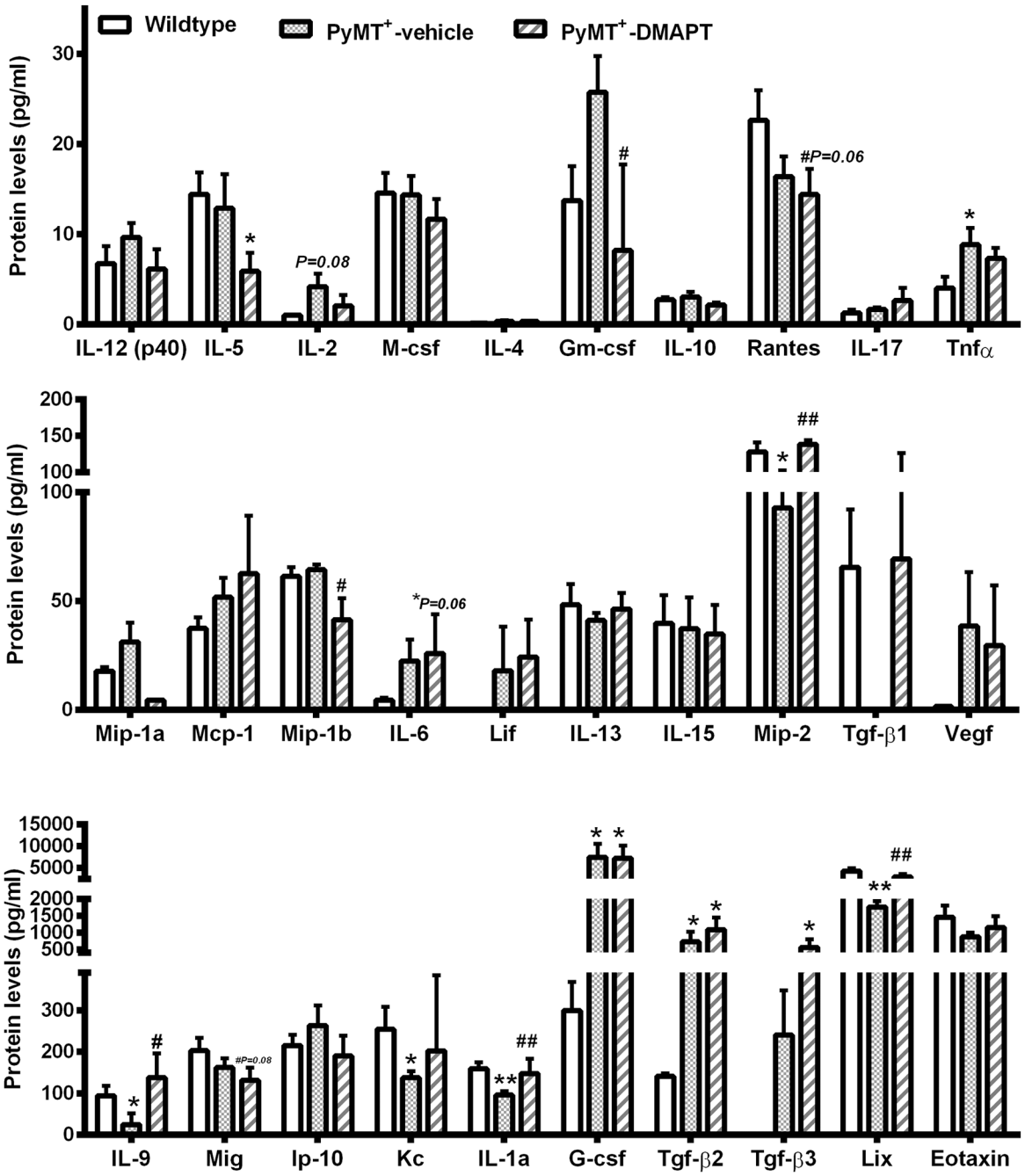

Figure 7.

DMAPT alters circulating levels of select cytokines/chemokines. Cytokine/chemokine levels were measured by multiplex ELISA using plasma from age-matched animals of three groups (n=6). A value of zero was given to cases with no detectable cytokine/chemokine content. Only data with at least three animals per group with detectable expression are included. Data are graphed as three panels based on cytokine/chemokine levels. * and ** indicates

significance between experimental and wild type groups, $p<0.05$; **p<0.001. # indicates significance between vehicle-treated and DMAPT-treated PyMT^{+} animals. $p<0.05$.